

# Mean-field study of the Bose-Hubbard model in Penrose lattice

Rasoul Ghadimi, Takanori Sugimoto, Takami Tohyama

*Department of Applied Physics, Tokyo University of Science, Tokyo 125-8585, Japan*

(Dated: October 11, 2021)

We examine the Bose-Hubbard model in the Penrose lattice based on inhomogeneous mean-field theory. Since averaged coordination number in the Penrose lattice is four, mean-field phase diagram consisting of the Mott insulator (MI) and superfluid (SF) phase is similar to that of the square lattice. However, the spatial distribution of Bose condensate in the SF phase is significantly different from uniform distribution in the square lattice. We find a fractal structure in its distribution near the MI-SF phase boundary. The emergence of the fractal structure is a consequence of cooperative effect between quasiperiodicity in the Penrose lattice and criticality at the phase transition.

## I. INTRODUCTION

Quasicrystals have aperiodic structure different from fully disordered one. Although translational symmetry is absent, the presence of sharp spots in Bragg reflection indicates long-range order [1, 2]. Quasicrystals can be realized even in bilayer graphene [3] and photonic lattices [4]. In addition to various characteristics due to aperiodicity [5, 6], recent new findings expand the field of quasicrystal to include superconductivity [7–10], quantum criticality [11, 12], and topology [13–17]. In general, self-similarity in quasicrystals dictates fractal structure in wavefunction and phase diagram [18, 19]. This characteristic is justified by the presence of the inflation and deflation rules to construct quasicrystals [20].

One of the well-known two-dimensional (2D) quasicrystals is the so-called Penrose lattice [21, 22]. One can construct the lattice using inflation, projection, or multi-grade rules. The Penrose lattice has been studied intensively [23–32] and its structure dictates thermodynamically degenerate states in energy spectrum [33, 34].

Ultracold gases in optical lattices provide us an ideal playground of strong correlation [35] and also quasicrystals [36–41], which allows us to investigate the interplay of strong correlation and aperiodicity. A typical strongly correlated system in optical lattice is the Bose-Hubbard model, where phase transition between Mott insulator (MI) to superfluid (SF) phase appears [42, 43] as experimentally observed [44, 45]. The Bose-Hubbard model is also used to describe the effective low-energy theory of superconducting films and arrays of Josephson junctions [46–48]. Recent achievements in establishing an eight-fold rotationally symmetric optical lattice attract new attention [49], in connection with theoretical investigation of an extended Bose-Hubbard with quasicrystalline confined potential [50], where spontaneous breaking of underlying eight-fold symmetry is observed. However, the effect of aperiodicity in the Bose-Hubbard model is not yet fully understood both theoretically and experimentally.

In this paper, we investigate the phase diagram of the Bose-Hubbard model in the Penrose lattice. We use a self-consistent mean-field theory and find that the distribution of Bose condensate in the Penrose lattice ex-

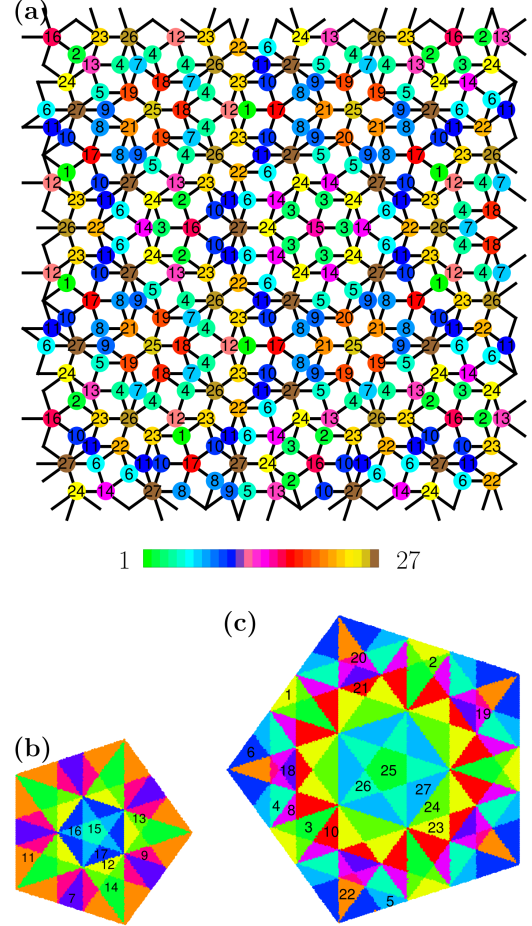


FIG. 1. (a) Part of Penrose lattice. The number and color in each vertex indicate the index  $\alpha$  of vertices among 27 different kinds of vertices. (b) Perpendicular space of Penrose lattice for  $Z = 1$ , and (c) that for  $Z = 2$ . The number is the same as (a). Different colors in (b) and (c) distinguish different sections in perpendicular space.

hibits a fractal structure near the MI-SF boundary. We attribute the appearance of the fractal structure to a consequence of the divergence of correlation length seen in any phase transition. Therefore, the fractal structure is a common signature of phase transition in quasiperiodic

TABLE I. Link configuration of distinct vertices in Penrose lattice. Listed are index  $\alpha$  determined in the present work, the total number of paths using  $k$  links,  $M_k$  ( $k = 1, 2, 3$ ), the number of vertices having  $l$  links, to which one can access using  $k$  links,  $m_k^{(l)}$  ( $l = 3, 4, 5, 6, 7$ ). Note that  $\sum_l m_k^{(l)} = M_k$ .

$\alpha$	1	2	3	4	5	6	7	8	9	10	11	12	13	14	15	16	17	18	19	20	21	22	23	24	25	26	27
$M_1$	3	3	3	3	3	3	3	3	3	3	3	4	4	4	5	5	5	5	5	5	5	5	5	5	5	6	7
$m_1^{(3)}$	0	0	0	0	0	0	0	0	0	0	0	2	2	2	5	5	5	4	4	4	4	4	3	2	0	3	6
$m_1^{(4)}$	0	0	0	1	1	1	0	0	0	0	0	0	0	0	0	0	0	0	0	0	0	0	1	2	0	0	0
$m_1^{(5)}$	3	3	3	1	1	1	2	2	2	2	2	2	2	2	0	0	0	1	1	1	1	0	0	0	5	3	1
$m_1^{(6)}$	0	0	0	1	0	0	1	0	0	0	0	0	0	0	0	0	0	0	0	0	0	1	1	0	0	0	0
$m_1^{(7)}$	0	0	0	0	1	1	0	1	1	1	1	0	0	0	0	0	0	0	0	0	0	0	0	1	0	0	0
$M_2$	15	15	15	15	16	16	16	17	17	17	17	16	16	16	15	15	15	17	17	17	17	18	19	21	25	24	23
$m_2^{(3)}$	11	10	9	9	12	12	11	15	14	14	13	6	5	4	0	0	0	0	0	0	0	3	5	10	20	10	2
$m_2^{(4)}$	2	3	4	0	0	0	0	0	0	1	1	4	5	6	0	0	0	2	2	2	0	2	0	0	0	4	4
$m_2^{(5)}$	0	0	0	6	4	3	5	2	3	1	1	2	2	2	15	13	11	11	11	11	13	9	12	11	5	4	10
$m_2^{(6)}$	2	1	0	0	0	1	0	0	0	1	2	4	2	0	0	0	0	4	2	0	0	0	0	0	0	6	0
$m_2^{(7)}$	0	1	2	0	0	0	0	0	0	0	0	0	2	4	0	2	4	0	2	4	4	4	2	0	0	0	7
$M_3$	53	55	57	57	56	57	58	55	57	57	60	68	71	74	75	79	83	87	89	91	93	90	89	85	85	102	121

systems.

The arrangement of this paper is as follows. In Sec. II, we describe our Bose-Hubbard model on the Penrose lattice and mean-field treatment. The classification of lattice sites (vertices) is also introduced. In Sec. III, we discuss the result of phase diagram, local superfluid amplitude, and a critical behavior of several quantities. A fractal structure near the phase transition in the perpendicular space in the Penrose lattice is also discussed. Finally, a summary is given in Sec. IV.

## II. MODEL AND METHOD

The Hamiltonian of the single-band Bose-Hubbard model is defined by

$$H_{BH} = -J \sum_{\langle i,j \rangle} (\hat{b}_i^\dagger \hat{b}_j + \hat{b}_j^\dagger \hat{b}_i) - \mu \sum_i \hat{n}_i + \frac{U}{2} \sum_i \hat{n}_i(\hat{n}_i - 1), \quad (1)$$

where  $\hat{b}_i$  and  $\hat{b}_i^\dagger$  are annihilation and creation operators of bosons at site  $i$  and the number operator  $\hat{n}_i = \hat{b}_i^\dagger \hat{b}_i$ . We refer the site to vertex, which is denoted by circles in Fig. 1(a). The summation  $\langle i, j \rangle$  represents nearest-neighbor (NN) links in the Penrose lattice shown as short bar connecting two vertices in Fig. 1(a).  $J$ ,  $\mu$ , and  $U$  in Eq. (1) are the hopping energy of boson, the chemical potential, and on-site Coulomb interaction, respectively. We note that hopping processes with the shortest inter-vertex distance, for example, hopping between numbers 8 and 9 in Fig. 1(a), are not included in Eq.(1). This exclusion guarantees bipartite properties of this Penrose lattice.

Because of the presence of the hopping term in Eq. (1), the exact solution is inaccessible. Therefore, we use a mean-field technique and decouple the hopping term using local superfluid amplitude  $\langle \hat{b}_i \rangle$ . The resulting mean-

field Hamiltonian is given by  $H_{MF} = \sum_i H_i + E_0$  with

$$H_i = -J \left( \psi_i^* \hat{b}_i + H.c. \right) - \mu \hat{n}_i + \frac{U}{2} \hat{n}_i(\hat{n}_i - 1), \quad (2)$$

where  $\psi_i = \sum_{j \in \text{NN}, i} \langle \hat{b}_j \rangle$  with summation over NN links connected to the vertex  $i$  and  $E_0 = J \sum_i \psi_i^* \langle \hat{b}_i \rangle$ .

In order to obtain a self-consistent solution of Eq. (2) in the local Hilbert space containing maximally  $n_b$  bosons, we start with an initial  $\psi_i$  and then calculate  $\langle \hat{n}_i \rangle$  and  $\langle \hat{b}_i \rangle$  using the ground-state wavefunction for each vertex. We continue updating  $\psi_i$  until the convergence of  $\langle \hat{n}_i \rangle$  and  $\langle \hat{b}_i \rangle$  is obtained within a certain tolerance ( $10^{-9}$  in our case). This self-consistent procedure gives rise to site-dependent distribution of  $\langle \hat{n}_i \rangle$  and  $\langle \hat{b}_i \rangle$  on the Penrose lattice. This technique is sometimes called inhomogeneous mean-field theory [51, 52], which gives equivalent results with variational Gutzwiller method [53–60]. We note that this self-consistent procedure gives moderately consistent results compared by quantum Monte Carlo simulations in determining the phase diagram of the Bose-Hubbard model with NN repulsion interaction [61].

We take  $n_b = 7$ . Within our mean-field theory, we generally find the MI and SF phases in the Bose-Hubbard model. In the MI phase, all sites have equal integer number of bosons and thus  $\langle \hat{b}_i \rangle = 0$ . On the other hand,  $\langle \hat{b}_i \rangle$  is nonzero for the SF phase. In our method, we find order parameters on all vertices. Therefore, we can check the existence of exotic states like Bose-glass, supersolid, and density-wave phases. We did not see these phases in our model. This is reasonable since these phases appear in the presence of disorder and/or NN interaction in Eq. (1) [52, 57, 62]. To minimize the boundary effects, we apply periodic boundary conditions (PBC) in an approximant of Penrose lattice containing  $N = 167761$  vertices (For detail, see the Appendix. A) [63–65].

In the Penrose lattice, we can classify vertices in terms

of their local environment. For this classification, we first find the number of NN links,  $M_1$ , i.e., the total number of paths using one link ( $M_k$  with  $k = 1$  and see the second row in Table I), which is equivalent to coordination number for each vertex in Fig. 1(a).  $M_1$  changes from 3 to 7. This means that all of sites are indexed by five kinds of vertices. Next, we count the number of NN vertices having  $l$  links,  $m_1^{(l)}$ , and make a list of them (the third-seventh rows in Table I). From the list of  $m_1^{(l)}$  together with  $M_1$ , we find fourteen types of configurations, meaning that all of sites are indexed by fourteen kinds of vertices. The total number of paths using two links ( $k = 2$ ) from a given vertex is then expressed as  $M_2 = \sum_{l=3}^7 m_1^{(l)} l$ , which is listed in the eighth row of Table I. We repeat this listing for the vertices accessed by using the two links form a given vertex, which is shown in the ninth-thirteenth rows as  $m_2^{(l)}$ . In the last row of Table I, the total number of paths using three links ( $k = 3$ ) from a given vertex ( $M_3 = \sum_{l=3}^7 m_2^{(l)} l$ ) is listed. Performing this procedure for all vertices in our supercell, we find that there are twenty-seven kinds of vertices, by which almost the whole system is covered. They are indexed as  $\alpha (= 1, 2, \dots, 27)$  in the first row of Table I. We note that, in our approximant periodic lattice with  $N = 167761$  vertices, there are vertices that do not belong to the 27 types around defects, but we can ignore them since the total number of the defects is just 2.

We call the number of distinct vertices for a given  $k$  the number of classes (NoC). For example, NoC is equal to 5, 14, and 27 for  $k = 1, 2$ , and 3, respectively. We draw a small portion of Penrose lattice in Fig. 1(a), where each vertex has an index  $\alpha (= 1, 2, \dots, 27)$  and color indicating its class obtained for  $k = 3$ . We can increase  $k$  as many as possible. We find  $\text{NoC} \propto k^{1.84}$  in the large  $k$  region (see Fig. 3(c)). We will come back to this point later.

As explained in the Appendix. A, vertexes in the Penrose lattice can be labeled with five integers, originated from cut and projection of five dimensional cubic lattice [28]. One can construct original Penrose lattice by mapping those labels. However, using another mapping, one finds four different 2D structures, called perpendicular space, where we assign the four structures to  $\mathcal{Z} = 1, 2, 3$ , and 4 [see Figs. 1(b) and 1(c) for  $\mathcal{Z} = 1$  and 2, respectively]. We can divide perpendicular space into symmetric sections, where each section represents vertex with similar local circumstances. Therefore, one notices the index  $\alpha$  in Fig. 1(a) mapped to different sections in the perpendicular space [see Figs. 1(b) and 1(c)]. We note that the bipartite property of Penrose lattice leads to the fact that  $\mathcal{Z} = 1, 3$  and  $\mathcal{Z} = 2, 4$  belong to different subsystems, though the same  $\alpha$  are shared among them.

### III. RESULTS

We first examine the phase diagram of the Bose-Hubbard model on the Penrose lattice. From the calcula-

tion of two order parameters per vertex,  $\langle \hat{n}_i \rangle$  and  $\langle \hat{b}_i \rangle$ , for the Bose-Hubbard model without disorder and/or inter-site interaction, we expect two phases: one is MI with  $\langle \hat{b}_i \rangle = 0$  and  $\langle \hat{n}_i \rangle = n_0$  ( $n_0 = 1, 2, \dots$ , corresponding to bosonic occupation number at each vertex), and the other is SF with  $\langle \hat{b}_i \rangle \neq 0$ . In fact, we find none of Bose-glass, density wave, and supersolid phases in the phase diagram. Figure 2 shows the phase diagram, where we find MI phases denoted by  $\text{MI}n_0$  and SF. Since averaged coordination number in the Penrose lattice is  $\bar{z} = 4$ , which is the same as the coordination number  $z = 4$  in the square lattice, the phase boundary between MI and SF is expected to be similar to that of the square lattice. This is the case as shown by the dashed orange curve along MI lobes in Fig. 2, which is mean-field phase boundary for the square lattice given analytically [66, 67] by

$$zJ_c/U = \frac{-\frac{\mu}{U} - (\frac{\mu}{U})^2 + s + 2\frac{\mu}{U}s - s^2}{1 + \frac{\mu}{U}}, \quad (3)$$

where  $s = \text{round}(\mu/U + 1/2)$ . The similarity indicates small effect of aperiodicity on the phase boundary.

In the SF phase of square lattice, the local superfluid amplitude  $\langle \hat{b}_i \rangle$  is uniform, i.e., independent of  $i$ , for any region in the phase diagram. On the other hand, nonuniform distribution of  $\langle \hat{b}_i \rangle$  in the Penrose lattice is easily expected from the presence of different types of vertices as shown in Fig. 1(a). Then, an arising question is how its nonuniform distribution changes in the phase diagram. To see this, we define an  $\alpha$  dependent average of  $\langle \hat{b}_i \rangle$  as  $\bar{b}_\alpha = N_\alpha^{-1} \sum_{i \in \alpha} \langle \hat{b}_i \rangle$ , where  $N_\alpha$  is the number of  $\alpha$ -type vertex in the whole lattice. This quantity can distinguish the twenty-seven classes of vertices. However, each class should have further internal structure coming from possible extension of NoC for  $k \geq 4$ . To recognize this structure, we also define a mean deviation of local superfluid amplitude distribution as  $\delta b_\alpha = \sqrt{N_\alpha^{-1} \sum_{i \in \alpha} (\langle \hat{b}_i \rangle - \bar{b}_\alpha)^2}$ .

With approaching phase transition from the superfluid side, the average value of local superfluid amplitude,  $\bar{b} = \sum_i \langle \hat{b}_i \rangle / N$  with  $N = \sum_\alpha N_\alpha$ , reduces its value toward zero as shown in the inset of Fig. 3(a). At the same time, both  $\bar{b}_\alpha$  and  $\delta b_\alpha$  become smaller. Therefore, we use  $\delta \bar{b}_\alpha / \bar{b}$  to evaluate the magnitude of the mean deviation of  $\delta b_\alpha$ . Note that the larger  $\delta b_\alpha / \bar{b}$  is, the deeper the internal structure is.

In Fig. 3(a), we plot  $\bar{b}_\alpha / \bar{b}$  and  $\delta b_\alpha / \bar{b}$  as a function of  $\bar{z}J/U$  along the horizontal dotted line ( $\mu/U = 0.8$ ) in Fig. 2. We note that  $\delta b_\alpha / \bar{b}$  is denoted by the length of bars for each  $\bar{b}_\alpha / \bar{b}$ . At large  $\bar{z}J/U$  far from the phase boundary,  $\bar{b}_\alpha / \bar{b}$  is tend to be grouped accompanied by negligibly small  $\delta b_\alpha / \bar{b}$ . In the limit of  $\bar{z}J/U \rightarrow \infty$ ,  $\bar{b}_\alpha / \bar{b}$  is grouped into five classes equivalent to the coordination number, i.e., NoC for  $k = 1$ . This means that, if correlation effect is small, the coordination number controls physical properties as expected. On the other hand, with approaching  $\bar{z}J/U$  to the phase boundary, the mean

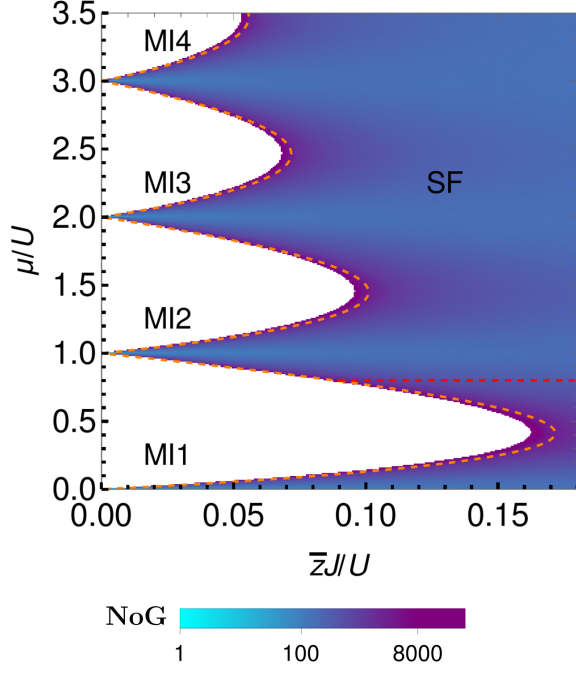


FIG. 2. Phase diagram of the Bose-Hubbard model on the Penrose lattice. The white area with the shape of lobes corresponds to the MI phase with  $n_0$  bosons in all vertices, denoted by  $MI n_0$  ( $n_0 = 1, 2, \dots$ ). In the SF phase, the number of gap (NoG) for a threshold value of  $10^{-7}$  defined in the text is plotted with color scale. The analytical MI-SF mean-field phase boundary for the square lattice in Eq. (3) is plotted by the orange dashed curve.

deviation  $\delta b_\alpha/\bar{b}$  becomes large. This means that the number of distinct vertices with different local superfluid amplitude increases with approaching to the boundary. In other words, long-distant correlation becomes important in order to obtain critical behaviors near the phase transition.

In order to make critical behaviors visible, we introduce a new quantity that can characterize distinct number of vertices more than twenty seven. We use  $\langle \hat{b}_i \rangle$  itself for this purpose, and try to find how many distinct values exist with approaching to the phase boundary. For distinguishing different value of local superfluid amplitude, we i) make shifting and scaling for  $\langle \hat{b}_i \rangle$  to be located within  $[0, 1]$ . This is done by evaluating  $(\langle \hat{b}_i \rangle - \min[\{\langle \hat{b}_i \rangle\}]) / (\max[\{\langle \hat{b}_i \rangle\}] - \min[\{\langle \hat{b}_i \rangle\}])$ , where min and max denote minimum and maximum among all values of local superfluid amplitude, respectively. Then, we ii) sort the scaled  $\langle \hat{b}_i \rangle$  from 0 to 1, iii) calculate the difference of  $\langle \hat{b}_i \rangle$  between  $i$  and  $i + 1$  from  $i = 1$  to  $i = N - 1$ , and iv) count the number of the difference (gap) whose magnitude is more than a given small threshold value. We call this number the number of gap (NoG). For example, NoG is zero for the square lattice because  $\langle \hat{b}_i \rangle$  is independent of  $i$ . In the Penrose lattice,

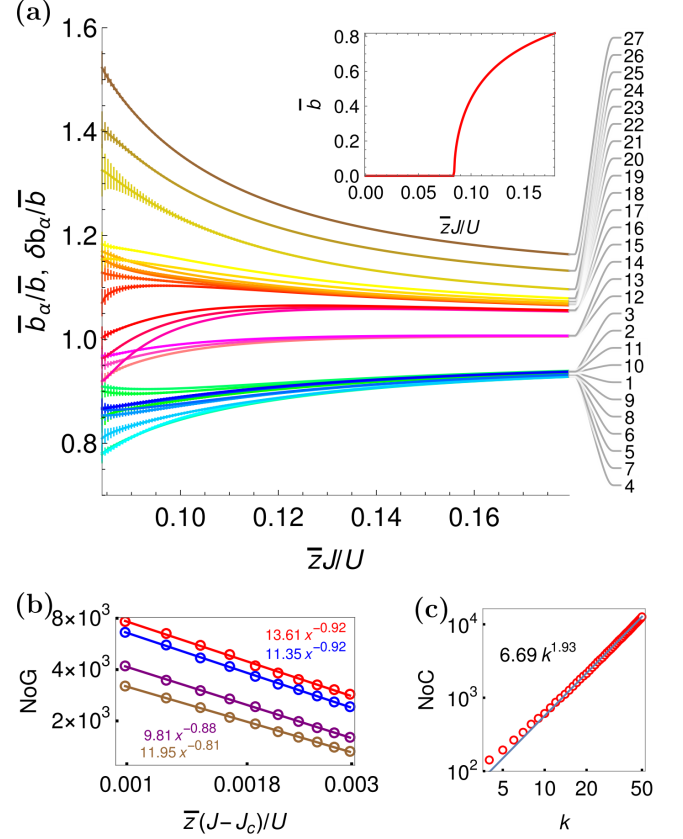


FIG. 3. (a) Averaged order parameters  $\bar{b}_\alpha/\bar{b}$  and mean deviation  $\delta b_\alpha/\bar{b}$  as a function of  $\bar{z}J/U$  along the horizontal dotted line ( $\mu/U = 0.8$ ) in Fig. 2. The colored curves represent  $\bar{b}_\alpha/\bar{b}$ . The bars centered at each curve represent  $\delta b_\alpha/\bar{b}$ . The color scheme is the same as Fig. 1(a) and the number denoted at the right-hand side indicates each class  $\alpha$  as shown in Fig. 1(a). Inset shows averaged order parameter  $\bar{b}$ . (b) Log-log plot of the number of gaps (NoG) defined in the text as a function of  $\bar{z}(J - J_c)/U$  along the horizontal dotted line in Fig. 2. The brown, purple, blue and red circles represent NoG for threshold values of  $10^{-5}$ ,  $5 \times 10^{-6}$ ,  $10^{-6}$ ,  $5 \times 10^{-7}$ , respectively. The lines represent fitting function denoted by the corresponding color, where  $x = \bar{z}(J - J_c)/U$ . (c) Log-log plot of the number of classes (NoC) as a function of the number of links  $k$ . The blue line represents a fitting function shown in the figure.

we have NoG = 4 in the large limit of  $\bar{z}J/U$  since there are five distinct values of  $\langle \hat{b}_i \rangle$ . We show log-log plot of NoG in Fig. 3(b) along the horizontal dotted line in Fig. 2, where four different threshold values,  $10^{-5}$ ,  $5 \times 10^{-6}$ ,  $10^{-6}$ , and  $5 \times 10^{-7}$  are used. With approaching to the phase boundary at  $\bar{z}J_c/U \approx 0.0835$ , NoG increases, indicating the increase of distinct vertices with different local superfluid amplitude. Interesting is that, with decreasing the threshold value, NoG rapidly increases near the boundary and shows a diverging behavior with an approximate exponent around  $-0.9$ , i.e.,  $\text{NoG} \propto (J - J_c)^{-0.9}$ . This resembles to a critical behavior toward continuous phase transition as suggested from the vanishing of averaged

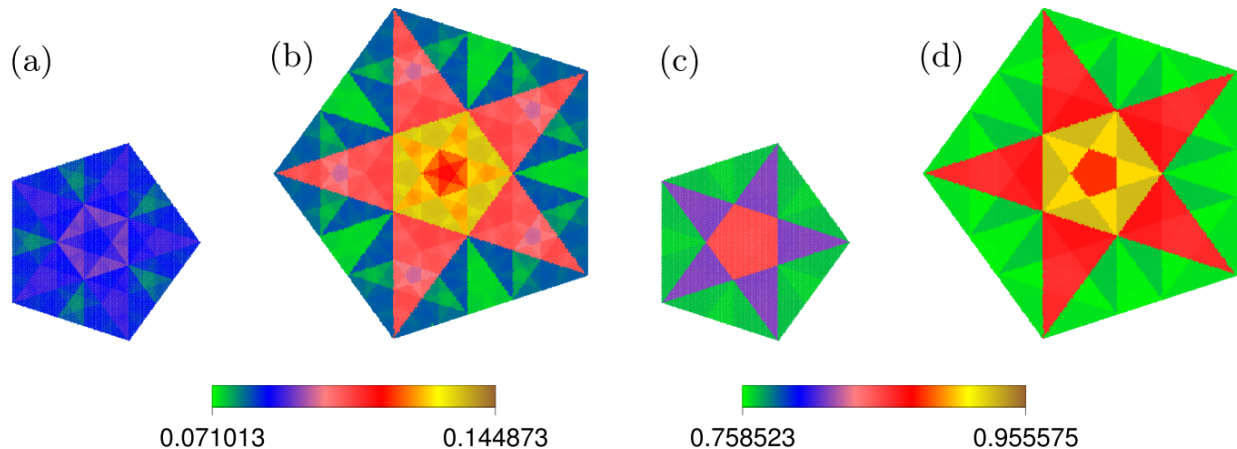


FIG. 4. Representation of vertex local superfluid amplitude in perpendicular space ( $\mathcal{Z} = 1, 2$ ) for (a,b)  $(\mu/U, \bar{z}J/U) = (0.8, 0.084)$  and for (c,d)  $(\mu/U, \bar{z}J/U) = (0.8, 0.18)$ . The numbers in color bars show extremes of local superfluid amplitude for given parameters.

order parameter  $\bar{b}$  [see inset of Fig 3(a)].

In order to understand this diverging behavior more, we focus on the fact that the increase of NoG corresponds to the increase of distinct vertices with different local superfluid amplitude. The latter is measured by NoC, whose large region is proportional to  $k^{1.84}$  as shown in Fig. 3(c). Therefore, diverging behavior in NoG is directly connected to diverging behavior in NoC at large  $k$ . Since  $k$  represents the number of links from a given vertex, we may regard  $k$  as a measure of correlation length  $\xi$  from a given vertex. Based on this reasoning, we have  $\text{NoG} \propto \text{NoC} \propto k^{1.84} \propto \xi^{1.84}$ . Since  $\xi \propto (J - J_c)^{-0.5}$  for the mean-field phase transition, we finally expect that  $\text{NoG} \propto (J - J_c)^{-0.92}$ , whose exponent is close to the calculated one in NoG,  $\approx -0.9$ . This indicates that diverging behavior in NoG is a consequence of criticality in the mean-field phase transition. We note that this critical behavior does not appear if  $\mu/U = n_0$  and  $J/U \rightarrow 0$ . We suggest that the assumption of  $\xi \propto k$  may change if we alter the class of universality. We leave this to future work.

Usefulness of perpendicular space presentation has already been found in considering magnetism on the Penrose lattice [25, 28]. Therefore, we show the perpendicular space representation of  $\langle \hat{b}_i \rangle$  in Fig. 4 for two sets of parameters at the end of the red dashed line in Fig. 2. We recognize notable differences in the two cases. For the parameter far from the phase boundary, we find fourteen distinct sections in Figs. 4(c) and 4(d). The number corresponds to the number of distinct vertices obtained by setting  $k = 2$  as discussed above. On the other hand, for the parameter close to the phase boundary, we can see a fractal structure in Figs. 4(a) and 4(b). For example, we find a various size of star structure inside stars. We can understand the emergence of the fractal structure near the phase transition as follows. Because of diverging behavior in NoG near the MI-SF phase boundary,

all distances become relevant. We have found from the previous discussion that tracing far distant links by increasing  $k$  enhances NoC dramatically. Therefore we can expect further distinguishable sections in the perpendicular space, resulting in fractal nature. In other words, a combination of criticality leading to phase transition and aperiodicity is a key for the emergence of fractal structure.

#### IV. CONCLUSION

We have obtained mean-field phase diagram in the Penrose-Bose-Hubbard model. We have found that the Penrose lattice does not change the MI-SF boundary drastically in comparison with square lattice. However, the spatial distribution of Bose condensate is unequal, and indeed fractal structure appears in the perpendicular representation of local superfluid amplitude near the MI-SF phase transition. This is a consequence of the co-operative effect of criticality leading to phase transition and quasiperiodicity, which is expected to be a common feature in aperiodic strongly correlated systems.

#### V. ACKNOWLEDGMENTS

This work was supported by Challenging Research Exploratory (Grant No. JP17K18764), Grant-in-Aid for Scientific Research on Innovative Areas (Grant No. JP19H05821).



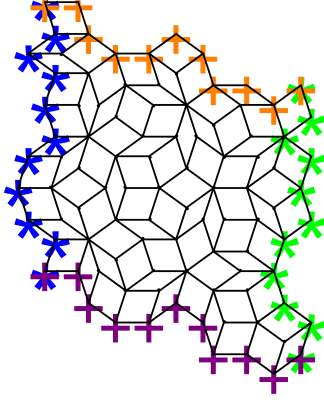


FIG. 5. An approximant of Penrose lattice with an approximated golden ratio  $\tau \approx \tau_3 = 3/2$ , including  $N_v = 76$  vertices in a unit cell. With periodic boundary condition, orange crosses on the upper (green stars on the right) boundaries are identified with purple crosses on the lower (blue stars on the left) boundaries.

#### Appendix A: Periodic boundary condition and perpendicular representation in Penrose lattice

In the appendix, we explain how to construct a two-dimensional finite-size Penrose lattice with periodic boundary condition systematically. To make a finite-size Penrose lattice, a cut-and-projection method is well known and established. In this method, we first consider a hypercubic lattice in a five-dimensional space consisting of two-dimensional real space and three-dimensional perpendicular space. Five primitive vectors of the hypercubic lattice are given by,

$$\mathbf{e}_i = (\delta_{i,1}, \delta_{i,2}, \delta_{i,3}, \delta_{i,4}, \delta_{i,5}) \quad (i = 1, 2, \dots, 5). \quad (\text{A1})$$

Thus, vertices on the hypercubic lattice are written by  $\mathbf{n}_k = \sum_{i=1}^5 n_{k,i} \mathbf{e}_i$ , where  $k$  is the vertex number and  $n_{k,i} \in \mathbb{Z}$ . Here, we introduce the real (perpendicular) space as two-dimensional plane (three-dimensional space) constructed by orthonormal vectors  $\mathbf{v}_1$  and  $\mathbf{v}_2$  ( $\mathbf{v}_3, \mathbf{v}_4$  and  $\mathbf{v}_5$ ) defined by

$$\mathbf{v}_1 = \sqrt{\frac{2}{5}} (1, \cos \phi, \cos 2\phi, \cos 3\phi, \cos 4\phi), \quad (\text{A2})$$

$$\mathbf{v}_2 = \sqrt{\frac{2}{5}} (0, \sin \phi, \sin 2\phi, \sin 3\phi, \sin 4\phi), \quad (\text{A3})$$

$$\mathbf{v}_3 = \sqrt{\frac{2}{5}} (1, \cos 2\phi, \cos 4\phi, \cos \phi, \cos 3\phi), \quad (\text{A4})$$

$$\mathbf{v}_4 = \sqrt{\frac{2}{5}} (0, \sin 2\phi, \sin 4\phi, \sin \phi, \sin 3\phi), \quad (\text{A5})$$

$$\mathbf{v}_5 = \sqrt{\frac{1}{5}} (1, 1, 1, 1, 1) \quad (\text{A6})$$

with  $\phi = 2\pi/5$ . Note that these vectors are orthonormal. To project five-dimensional vertices into the real

and perpendicular spaces, we use projection matrices,

$$\mathbf{P}_r = \sum_{i=1}^2 \mathbf{e}_i^{(r)} \otimes \mathbf{v}_i, \quad \mathbf{P}_p = \sum_{j=1}^3 \mathbf{e}_j^{(p)} \otimes \mathbf{v}_{j+2}, \quad (\text{A7})$$

where unit vectors in real and perpendicular spaces are given by  $\mathbf{e}_i^{(r)} = (\delta_{i,1}, \delta_{i,2})_r$  and  $\mathbf{e}_j^{(p)} = (\delta_{j,1}, \delta_{j,2}, \delta_{j,3})_p$  for  $i = 1, 2$  and  $j = 1, 2, 3$ , respectively. By using the projection matrices, the real- and perpendicular-space vertices are obtained by  $\mathbf{v}_k^{(r)} = \mathbf{P}_r \mathbf{n}_k = (\mathbf{n}_k \cdot \mathbf{v}_1, \mathbf{n}_k \cdot \mathbf{v}_2)_r$  and  $\mathbf{v}_k^{(p)} = \mathbf{P}_p \mathbf{n}_k = (\mathbf{n}_k \cdot \mathbf{v}_3, \mathbf{n}_k \cdot \mathbf{v}_4, \mathbf{n}_k \cdot \mathbf{v}_5)_p$ . As confirmed easily, we can find all vertices in a Penrose lattice as the vertices of hypercubic lattice projected into the real space, e.g., five vertices  $\mathbf{n}_k = \mathbf{e}_k$  for  $k = 1, 2, \dots, 5$  give five apices of pentagon (star) located on the origin.

However, the projected vertices obviously include unwanted vertices for a Penrose lattice. To exclude these unwanted vertices, we use a three-dimensional window in the perpendicular space. The window is a rhombic icosahedron constructed by five vectors  $\mathbf{d}_i^{(p)} = \mathbf{P}_p \mathbf{e}_i$ ; inner space of the window is given by  $\mathcal{W} = \left\{ \sum_{i=1}^5 r_i \mathbf{d}_i^{(p)} \mid r_i \in [0, 1] \right\}$ . If a projected vertex into the perpendicular space  $\mathbf{P}_p \mathbf{n}_k$  is out of the window, we ignore a projected vertex of  $\mathbf{n}_k$  into the real space. Through this procedure, we exclude the unwanted vertices for a Penrose lattice [68]. Note that the allowed vertices  $\mathbf{n}_k$  are classified into four groups by an integer index  $Z = \sqrt{5} \mathbf{n}_k \cdot \mathbf{v}_5 = 1, 2, 3, 4$  corresponding to  $z$  component of the perpendicular space, i.e., four planes in the perpendicular space. Therefore, the four planes restricted in the window include all vertices giving a Penrose lattice.

Next, we move to a Penrose lattice with periodic boundary condition, which corresponds to an approximant of Penrose lattice. To obtain the approximant, we use a multigrid method as follows [64]. In this method, we make a Penrose lattice or its approximant in two steps: (i) find a five-dimensional integer vector  $\mathbf{n}(\mathbf{x})$  as a function of two-dimensional real vector  $\mathbf{x}$ , and (ii) make a vertex of the Penrose lattice or its approximant with  $\mathbf{v}^{(r)}(\mathbf{x}) = \mathbf{P}_r \mathbf{n}(\mathbf{x}) = \sum_{i=1}^5 n_i(\mathbf{x}) \mathbf{d}_i^{(r)}$  where  $\mathbf{d}_i^{(r)} = \mathbf{P}_r \mathbf{e}_i$ . As explained above, if the integer vector  $\mathbf{n}(\mathbf{x})$  includes all vectors consisting of arbitrary integers  $n_i \in \mathbb{Z}$ , unwanted vertices are also included in a Penrose lattice obtained by the step (ii) with  $\mathbf{n}(\mathbf{x})$ . To exclude unwanted vertices, interestingly, we only consider the integer vector given by

$$n_i(\mathbf{x}) = \lfloor \mathbf{x} \cdot \mathbf{d}_i^{(r)} - \gamma_i \rfloor, \quad (\text{A8})$$

where the floor function  $\lfloor a \rfloor$  denotes the largest integer less than or equal to  $a$ , and  $\gamma_i$  is an arbitrary real number satisfying  $\sum_{i=1}^5 \gamma_i \in \mathbb{Z}$ . In this equation, the floor function gives an integer indexing a neighboring vertex of  $\mathbf{x}$ , and  $\gamma_i$  plays the role of window [65]. Therefore, if we search all integer vectors  $\mathbf{n}(\mathbf{x})$  in a two-dimensional certain finite space  $\mathbf{x} \in \mathcal{S}_r$ , we can obtain a finite-size

Penrose lattice around the space  $\mathcal{S}_r$ . However, this procedure usually requires a careful searching without dropping any vertices. To find the set of integer vectors  $\mathbf{n}(\mathbf{x})$  efficiently, we use a recursive algorithm proposed in Ref. [69].

On the other hand, to approximate the Penrose lattice to a periodic lattice, we substitute in Eq. (A8) for the quasi unit vectors  $\mathbf{d}_i^{(r)}$  rewritten by,

$$\begin{aligned} \mathbf{d}_1^{(r)} &= \sqrt{\frac{2}{5}}(1, 0)_r, \\ \mathbf{d}_2^{(r)} &= \sqrt{\frac{2}{5}}(\cos \phi, \sin \phi)_r, \\ \mathbf{d}_3^{(r)} &= -\mathbf{d}_1^{(r)} + \tau^{-1}\mathbf{d}_2^{(r)}, \\ \mathbf{d}_4^{(r)} &= -\tau^{-1}\left\{\mathbf{d}_1^{(r)} + \mathbf{d}_2^{(r)}\right\}, \\ \mathbf{d}_5^{(r)} &= \tau^{-1}\mathbf{d}_1^{(r)} - \mathbf{d}_2^{(r)}. \end{aligned} \quad (\text{A9})$$

Here, the golden ratio  $\tau = (1 + \sqrt{5})/2$  is approximated by a rational number  $\tau_n \equiv F_{n+1}/F_n \xrightarrow{n \rightarrow \infty} \tau$ , where  $F_n$  is the  $n$ th Fibonacci number. With the rational number  $\tau_n$ , the quasi unit vectors give a large unit cell with translational symmetry. Therefore, we obtain an approximant of Penrose lattice as the unit cell including  $N_v = 4F_{2n+1} + 3F_{2n}$  vertices. Figure 5 represents an approximant with  $n = 3$ , which contains  $N_v = 76$  vertices as a unit cell. Note that the upper (right) and lower (left) boundaries of this approximant are connected with periodic boundary condition. In this paper, we consider an approximant of Penrose lattice with  $n = 11$ , which results in  $N_v = 167761$  vertices at most.

- 
- [1] D. Shechtman, I. Blech, D. Gratias, and J. W. Cahn, “Metallic phase with long-range orientational order and no translational symmetry,” *Phys. Rev. Lett.* **53**, 1951–1953 (1984).
  - [2] Dov Levine and Paul Joseph Steinhardt, “Quasicrystals: A new class of ordered structures,” *Phys. Rev. Lett.* **53**, 2477–2480 (1984).
  - [3] Wei Yao, Eryin Wang, Changhua Bao, Yiou Zhang, Kenan Zhang, Kejie Bao, Chun Kai Chan, Chaoyu Chen, Jose Avila, Maria C. Asensio, Junyi Zhu, and Shuyun Zhou, “Quasicrystalline 30° twisted bilayer graphene as an incommensurate superlattice with strong interlayer coupling,” *Proceedings of the National Academy of Sciences* **115**, 6928–6933 (2018).
  - [4] Wentao Jin and Yuanmei Gao, “Optically induced two-dimensional photonic quasicrystal lattices in iron-doped lithium niobate crystal with an amplitude mask,” *Applied Physics Letters* **101**, 141104 (2012).
  - [5] Walter Steurer, “Quasicrystals: What do we know? What do we want to know? What can we know?” *Acta Crystallographica Section A* **74**, 1–11 (2018).
  - [6] D.V. Louzguine-Luzgin and A. Inoue, “Formation and properties of quasicrystals,” *Annual Review of Materials Research* **38**, 403–423 (2008).
  - [7] K. Kamiya, T. Takeuchi, N. Kabeya, N. Wada, T. Ishimasa, A. Ochiai, K. Deguchi, K. Imura, and N. K. Sato, “Discovery of superconductivity in quasicrystal,” *Nature Communications* **9**, 154 (2018).
  - [8] Ronaldo N. Araújo and Eric C. Andrade, “Conventional superconductivity in quasicrystals,” *Phys. Rev. B* **100**, 014510 (2019).
  - [9] Shiro Sakai, Nayuta Takemori, Akihisa Koga, and Ryotaro Arita, “Superconductivity on a quasiperiodic lattice: Extended-to-localized crossover of cooper pairs,” *Phys. Rev. B* **95**, 024509 (2017).
  - [10] Shiro Sakai and Ryotaro Arita, “Exotic pairing state in quasicrystalline superconductors under a magnetic field,” *Phys. Rev. Research* **1**, 022002 (2019).
  - [11] Kazuhiko Deguchi, Shuya Matsukawa, Noriaki K. Sato, Taisuke Hattori, Kenji Ishida, Hiroyuki Takakura, and Tsutomu Ishimasa, “Quantum critical state in a magnetic quasicrystal,” *Nature Materials* **11**, 1013–1016 (2012).
  - [12] Junya Otsuki and Hiroaki Kusunose, “Distributed hybridization model for quantum critical behavior in magnetic quasicrystals,” *Journal of the Physical Society of Japan* **85**, 073712 (2016).
  - [13] Li-Jun Lang, Xiaoming Cai, and Shu Chen, “Edge states and topological phases in one-dimensional optical superlattices,” *Phys. Rev. Lett.* **108**, 220401 (2012).
  - [14] Fuyuki Matsuda, Masaki Tezuka, and Norio Kawakami, “Topological properties of ultracold bosons in one-dimensional quasiperiodic optical lattice,” *Journal of the Physical Society of Japan* **83**, 083707 (2014).
  - [15] A. Dareau, E. Levy, M. Bosch Aguilera, R. Bouganne, E. Akkermans, F. Gerbier, and J. Beugnon, “Revealing the topology of quasicrystals with a diffraction experiment,” *Phys. Rev. Lett.* **119**, 215304 (2017).
  - [16] Stephen Spurrier and Nigel R. Cooper, “Theory of quantum oscillations in quasicrystals: Quantizing spiral fermi surfaces,” *Phys. Rev. B* **100**, 081405 (2019).
  - [17] Huaqing Huang and Feng Liu, “Quantum spin hall effect and spin bott index in a quasicrystal lattice,” *Phys. Rev. Lett.* **121**, 126401 (2018).
  - [18] Rasoul Ghadimi, Takanori Sugimoto, and Takami Tohyama, “Majorana zero-energy mode and fractal structure in fibonacci-kitaev chain,” *Journal of the Physical Society of Japan* **86**, 114707 (2017).
  - [19] Miguel A. Bandres, Mikael C. Rechtsman, and Mordechai Segev, “Topological photonic quasicrystals: Fractal topological spectrum and protected transport,” *Phys. Rev. X* **6**, 011016 (2016).
  - [20] Penghui Ma and Youyan Liu, “Inflation rules, band structure, and localization of electronic states in a two-dimensional penrose lattice,” *Phys. Rev. B* **39**, 9904–9911 (1989).
  - [21] N.G. de Bruijn, “Algebraic theory of penrose’s non-periodic tilings of the plane. i,” *Indagationes Mathematicae*

- icae (Proceedings) **84**, 39 – 52 (1981).
- [22] N.G. de Bruijn, “Algebraic theory of penrose’s non-periodic tilings of the plane. ii,” *Indagationes Mathematicae (Proceedings)* **84**, 53 – 66 (1981).
- [23] J Oitmaa, M Aydin, and M J Johnson, “Antiferromagnetic ising model on the penrose lattice,” *Journal of Physics A: Mathematical and General* **23**, 4537 (1990).
- [24] Youyan Liu and Penghui Ma, “Electronic properties of two-dimensional quasicrystals with near-neighbor interactions,” *Phys. Rev. B* **43**, 1378–1384 (1991).
- [25] Attila Szallas and Anuradha Jagannathan, “Spin waves and local magnetizations on the penrose tiling,” *Phys. Rev. B* **77**, 104427 (2008).
- [26] Patrizia Vignolo, Matthieu Bellec, Julian Böhm, Abdoulaye Camara, Jean-Marc Gambaudo, Ulrich Kuhl, and Fabrice Mortessagne, “Energy landscape in a penrose tiling,” *Phys. Rev. B* **93**, 075141 (2016).
- [27] Nayuta Takemori and Akihisa Koga, “DMFT study of the local correlation effects in quasi-periodic system,” *Journal of Physics: Conference Series* **592**, 012038 (2015).
- [28] Akihisa Koga and Hirokazu Tsunetsugu, “Antiferromagnetic order in the hubbard model on the penrose lattice,” *Phys. Rev. B* **96**, 214402 (2017).
- [29] Nayuta Takemori, Akihisa Koga, and Hartmut Hafermann, “Intersite electron correlations on inhomogeneous lattices: a real-space dual fermion approach,” (2018), arXiv:1801.02441 [cond-mat.str-el].
- [30] A. Jagannathan, “Quasiperiodic heisenberg antiferromagnets in two dimensions,” *The European Physical Journal B* **85**, 68 (2012).
- [31] Attila Szallas, Anuradha Jagannathan, and Stefan Wessel, “Phason-disordered two-dimensional quantum antiferromagnets,” *Phys. Rev. B* **79**, 172406 (2009).
- [32] Yuta Murakami, Denis Golež, Tatsuya Kaneko, Akihisa Koga, Andrew J. Millis, and Philipp Werner, “Collective modes in excitonic insulators: Effects of electron-phonon coupling and signatures in the optical response,” *Phys. Rev. B* **101**, 195118 (2020).
- [33] Masao Arai, Tetsuji Tokihiro, Takeo Fujiwara, and Mahito Kohmoto, “Strictly localized states on a two-dimensional penrose lattice,” *Phys. Rev. B* **38**, 1621–1626 (1988).
- [34] Takeo Fujiwara, Masao Arai, Tetsuji Tokihiro, and Mahito Kohmoto, “Localized states and self-similar states of electrons on a two-dimensional penrose lattice,” *Phys. Rev. B* **37**, 2797–2804 (1988).
- [35] Immanuel Bloch, “Ultracold quantum gases in optical lattices,” *Nature Physics* **1**, 23–30 (2005).
- [36] K. Singh, K. Saha, S. A. Parameswaran, and D. M. Weld, “Fibonacci optical lattices for tunable quantum quasicrystals,” *Phys. Rev. A* **92**, 063426 (2015).
- [37] L. Guidoni, C. Triché, P. Verkerk, and G. Grynberg, “Quasiperiodic optical lattices,” *Phys. Rev. Lett.* **79**, 3363–3366 (1997).
- [38] L. Sanchez-Palencia and L. Santos, “Bose-einstein condensates in optical quasicrystal lattices,” *Phys. Rev. A* **72**, 053607 (2005).
- [39] Theodore A. Corcovilos and Jahnavee Mittal, “Two-dimensional optical quasicrystal potentials for ultracold atom experiments,” *Appl. Opt.* **58**, 2256–2263 (2019).
- [40] Junpeng Hou, Haiping Hu, Kuei Sun, and Chuanwei Zhang, “Superfluid-quasicrystal in a bose-einstein condensate,” *Phys. Rev. Lett.* **120**, 060407 (2018).
- [41] Sarang Gopalakrishnan, Ivar Martin, and Eugene A. Demler, “Quantum quasicrystals of spin-orbit-coupled dipolar bosons,” *Phys. Rev. Lett.* **111**, 185304 (2013).
- [42] Matthew P. A. Fisher, Peter B. Weichman, G. Grinstein, and Daniel S. Fisher, “Boson localization and the superfluid-insulator transition,” *Phys. Rev. B* **40**, 546–570 (1989).
- [43] Omjyoti Dutta, Mariusz Gajda, Philipp Hauke, Maciej Lewenstein, Dirk-Sören Lühmann, Boris A Malomed, Tomasz Sowiński, and Jakub Zakrzewski, “Non-standard hubbard models in optical lattices: a review,” *Reports on Progress in Physics* **78**, 066001 (2015).
- [44] D. Jaksch, C. Bruder, J. I. Cirac, C. W. Gardiner, and P. Zoller, “Cold bosonic atoms in optical lattices,” *Phys. Rev. Lett.* **81**, 3108–3111 (1998).
- [45] Markus Greiner, Olaf Mandel, Tilman Esslinger, Theodor W. Hänsch, and Immanuel Bloch, “Quantum phase transition from a superfluid to a mott insulator in a gas of ultracold atoms,” *Nature* **415**, 39–44 (2002).
- [46] Thierry Giamarchi, Christian Rüegg, and Oleg Tchernyshyov, “Bose-einstein condensation in magnetic insulators,” *Nature Physics* **4**, 198–204 (2008).
- [47] T. Nikuni, M. Oshikawa, A. Oosawa, and H. Tanaka, “Bose-einstein condensation of dilute magnons in  $\text{tlcucl}_3$ ,” *Phys. Rev. Lett.* **84**, 5868–5871 (2000).
- [48] C. Bruder, Rosario Fazio, and Gerd Schön, “Superconductor-mott-insulator transition in bose systems with finite-range interactions,” *Phys. Rev. B* **47**, 342–347 (1993).
- [49] Konrad Viebahn, Matteo Sbroscia, Edward Carter, Jr-Chiun Yu, and Ulrich Schneider, “Matter-wave diffraction from a quasicrystalline optical lattice,” *Phys. Rev. Lett.* **122**, 110404 (2019).
- [50] Dean Johnstone, Patrik Öhberg, and Callum W. Duncan, “Mean-field phases of an ultracold gas in a quasicrystalline potential,” *Phys. Rev. A* **100**, 053609 (2019).
- [51] Ramesh V. Pai, Jamshid Moradi Kurdestany, K. Sheshadri, and Rahul Pandit, “Bose-hubbard models in confining potentials: Inhomogeneous mean-field theory,” *Phys. Rev. B* **85**, 214524 (2012).
- [52] J.M. Kurdestany, R.V. Pai, and R. Pandit, “The inhomogeneous extended bose-hubbard model: A mean-field theory,” *Annalen der Physik* **524**, 234–244 (2012), <https://onlinelibrary.wiley.com/doi/pdf/10.1002/andp.201100274>.
- [53] P. Pisarski, R. M. Jones, and R. J. Gooding, “Application of a multisite mean-field theory to the disordered bose-hubbard model,” *Phys. Rev. A* **83**, 053608 (2011).
- [54] T. McIntosh, P. Pisarski, R. J. Gooding, and E. Zaremba, “Multisite mean-field theory for cold bosonic atoms in optical lattices,” *Phys. Rev. A* **86**, 013623 (2012).
- [55] Apurba Barman and Saurabh Basu, “Phase diagram of trapped bosons in a kagome lattice—application of inhomogeneous mean field theory,” *Journal of Physics B: Atomic, Molecular and Optical Physics* **47**, 025302 (2014).
- [56] S. Yi, T. Li, and C. P. Sun, “Novel quantum phases of dipolar bose gases in optical lattices,” *Phys. Rev. Lett.* **98**, 260405 (2007).
- [57] K. Sheshadri, H. R. Krishnamurthy, Rahul Pandit, and T. V. Ramakrishnan, “Percolation-enhanced localization in the disordered bosonic hubbard model,” *Phys. Rev. Lett.* **75**, 4075–4078 (1995).



- [58] A. E. Niederle and H. Rieger, “Bosons in a two-dimensional bichromatic quasiperiodic potential: Analysis of the disorder in the bose-hubbard parameters and phase diagrams,” *Phys. Rev. A* **91**, 043632 (2015).
- [59] Daniel S. Rokhsar and B. G. Kotliar, “Gutzwiller projection for bosons,” *Phys. Rev. B* **44**, 10328–10332 (1991).
- [60] Werner Krauth, Michel Caffarel, and Jean-Philippe Bouchaud, “Gutzwiller wave function for a model of strongly interacting bosons,” *Phys. Rev. B* **45**, 3137–3140 (1992).
- [61] Takahiro Ohgoe, Takafumi Suzuki, and Naoki Kawashima, “Ground-state phase diagram of the two-dimensional extended bose-hubbard model,” *Phys. Rev. B* **86**, 054520 (2012).
- [62] M. Iskin, “Route to supersolidity for the extended bose-hubbard model,” *Phys. Rev. A* **83**, 051606 (2011).
- [63] O Entin-Wohlman, M Kléman, and A Pavlovitch, “Penrose tiling approximants,” *Journal de Physique* **49**, 587–598 (1988).
- [64] F. Babalievski and O. Peshev, “An algorithm to construct quasilattices and study percolation on them,” *Computer Physics Communications* **60**, 27 – 30 (1990).
- [65] Hirokazu Tsunetsugu, Takeo Fujiwara, Kazuo Ueda, and Tetsuji Tokihiro, “Electronic properties of the penrose lattice. i. energy spectrum and wave functions,” *Phys. Rev. B* **43**, 8879–8891 (1991).
- [66] D. van Oosten, P. van der Straten, and H. T. C. Stoof, “Quantum phases in an optical lattice,” *Phys. Rev. A* **63**, 053601 (2001).
- [67] J. K. Freericks and H. Monien, “Phase diagram of the bose-hubbard model,” *Europhysics Letters (EPL)* **26**, 545–550 (1994).
- [68] Marjorie Senechal, *Quasicrystals and geometry* (cambridge university press, 1996).
- [69] F.V Babalievski, “Percolation conductivity of penrose lattices by the transfer-matrix monte carlo method,” *Journal of Non-Crystalline Solids* **153-154**, 370 – 374 (1993), proceddings of the Fourth International Conference on Quasicrystals.